

Title : Fragment-based screening identifies inhibitors of the ATPase activity and of hexamer formation of Cag α from the *Helicobacter pylori* type IV secretion system

Authors : Tarun Arya, Flore Oudouhou, Bastien Casu, Benoit Bessette, Jurgen Sygusch and Christian Baron*

Affiliation : Department of Biochemistry and Molecular Medicine, Faculty of Medicine, Université de Montréal, Québec, Canada

***Corresponding Author:** E-mail: christian.baron@umontreal.ca

Keywords: Type IV secretion, fragment-based screening, enzyme inhibitors, drug design, stomach cancer, ulcer disease, anti-virulence drug, antimicrobial resistance

Abstract

Type IV secretion systems are membrane-bound multiprotein complexes that mediate the translocation of macromolecules across the bacterial cell envelope. In *Helicobacter pylori* a type IV secretion system is encoded by the *cag* pathogenicity island that encodes 27 Cag proteins and most of these are essential for bacterial virulence. We here present our work on the identification and characterization of inhibitors of Cag α , a hexameric ATPase and member of the family of VirB11-like proteins that is essential for translocation of the CagA cytotoxin into mammalian cells. We conducted fragment-based screening using a differential scanning fluorimetry assay and identified 16 molecules that stabilize the protein during thermal denaturation suggesting that they bind Cag α . Several of these molecules affect binding of ADP and four of them inhibit the ATPase enzyme activity of Cag α . Analysis of enzyme kinetics suggests that their mode of action is non-competitive, suggesting that they do not bind to the ATPase active site. Cross-linking analysis suggests that the active molecules change the conformation of the protein and gel filtration and transmission electron microscopy show that molecule 1G2 dissociates the Cag α hexamer. Analysis by X-ray crystallography reveals that molecule 1G2 binds at the interface between Cag α subunits. Addition of the molecule 1G2 inhibits the induction of interleukin-8 production in gastric cancer cells after co-incubation with *H. pylori* suggesting that it inhibits Cag α *in vivo*. Our results reveal a novel mechanism for the inhibition of the ATPase activity of VirB11-like proteins and the identified molecules have potential for the development into anti-virulence drugs.

Author summary

We here report the results of a small-molecule screening approach to identify inhibitors of an essential virulence factor from the gastrointestinal pathogen *Helicobacter pylori*. We identified novel chemical entities that bind to the Cag α protein and inhibit its function. We discovered a novel inhibitor binding site that disrupts the hexameric quaternary structure and inhibits ATPase enzyme activity of Cag α . Based on the structural information on the binding site, these molecules could be developed into high-affinity inhibitors that may have potential as anti-virulence drugs. This approach represents a generally applicable strategy for the inhibition of bacterial virulence factors for which structural information is available that could be applied to target similar proteins from many bacterial pathogens.

Introduction

Helicobacter pylori is a widespread pathogenic bacterium that lives in the stomach of over half of the world's population [1]. The infection with virulent strains causes inflammatory reactions, gastritis, peptic ulcers and it is one of the principal causes of stomach cancer in humans [2, 3]. Antibiotic treatments using combination therapies of three or four drugs have generally been successful, but eradication therapy is becoming increasingly difficult due to rising resistance against many antimicrobial agents, such as clarithromycin and metronidazole [4]. Novel treatment options are therefore urgently needed and targeting bacterial virulence factors to attenuate the inflammation is a strategy that could complement or even replace currently used eradication treatments.

Type IV secretion systems (T4SS) mediate the transfer of virulence factors across the cell envelope of many bacterial pathogens as well as the exchange of plasmids contributing to the spread of antibiotic resistance genes [5, 6]. *H. pylori* strains encode T4SSs that mediate the uptake of DNA as well as bacterial virulence like the *cag* pathogenicity island (*cag*-PAI)-encoded T4SS comprising 27 components of which most are essential for bacterial virulence [7-10]. The *cag*-PAI is required for the transfer of the CagA cytotoxin into mammalian cells where it is phosphorylated by Src kinase at tyrosine residues and its interactions with mammalian proteins such as SHP-2 and Grb-2 lead to rearrangements of the cytoskeleton and to proinflammatory reactions [11]. The *cag*-PAI-encoded T4SS is also a conduit for bacterial murein and for the small molecule metabolite heptulose-1,7-bisphosphate triggering signalling cascades via Nod-1 and TIFA, respectively, that contribute to the proinflammatory response [12, 13].

The *H. pylori* *cag*-PAI encodes 27 proteins including homologs of all 12 components of the

most studied model T4SS from *Agrobacterium tumefaciens* [9]. These conserved proteins are critical for secretion system function and they are either part of surface-exposed pili, of the periplasmic T4SS core complex or they energize T4SS assembly or substrate translocation. We here focus on the Cag α (HP0525) protein that is a member of the VirB11 family of ATPases present in all T4SSs. Electron microscopic (EM) analyses and X-ray crystallography have shown that the overall structures of VirB11-like proteins from different organisms are very similar comprising homo-hexameric rings [14, 15]. The monomeric subunit consists of an N-terminal domain (NTD) and a C-terminal domain (CTD) that are linked via a short linker region comprising the nucleotide binding site. The X-ray structures of Cag α apoprotein [16], as well as of its complexes with ADP [17] and with the inhibitor ATP γ S [16] have been solved. These studies revealed that the CTD forms a ‘six clawed grapple’ mounted onto the NTD, forming a hexameric ring and a dome-like chamber that is closed at one end and opened at the other [17]. Glycerol gradient centrifugation showed a large conformational change of VirB11 homologs from plasmid RP4 (TrbB) and *H. pylori* upon binding to ATP, underlining the dynamic nature of the protein [16, 18]. The other available X-ray structure from *Brucella suis* VirB11 differs from Cag α by a domain swap of the large linker region between NTD and CTD [19], but the overall structure is very similar.

Since T4SS are important for bacterial virulence they are very interesting targets for the development of drugs that disarm but do not kill bacterial pathogens [20, 21]. In our previous work, we have identified inhibitors of the dimerization of VirB8-like proteins from *B. suis* and plasmid pKM101 using the bacterial two-hybrid system and fragment-based screening approaches and we identified molecules that reduce T4SS function [22-25]. Other groups have identified peptidomimetic inhibitors of the *H. pylori* T4SS, but the targets of these molecules are not known [26]. Certain unsaturated fatty acids inhibit bacterial conjugation and the ATPase activity of the VirB11 homolog TrwD from plasmid

R388, but there is no high-resolution structural information available on their binding site [27, 28]. High-throughput small molecule screening and chemical synthesis led to the identification of inhibitors of the ATPase activity of Cag α that likely bind at the ATPase active site, but structural information on their binding site is not available [29, 30]. Whereas the isolation of competitive inhibitors of the ATPase activity of VirB11 homologs is interesting, there are concerns about the specificity of these molecules since they may also inhibit other ATPases in bacteria or in mammalian cells.

To identify novel chemical entities that inhibit Cag α we here present an unbiased approach that does not specifically target its ATPase activity. To this effect, we carried out fragment based-screening using differential scanning fluorimetry (DSF) to identify molecules that bind and stabilize Cag α [31]. Four of the molecules inhibit the Cag α ATPase activity and the most potent molecule impacts the conformation of the protein and dissociates the hexamer. X-ray crystallography reveals that this molecule causes conformational changes, that it binds at the interface between Cag α monomers and it inhibits the production of interleukin-8 upon interaction between *H. pylori* and mammalian cells.

Results

Differential scanning fluorimetry to identify Cag α -binding fragments

To identify novel chemical entities that bind to and influence the activity of Cag α , we conducted fragment-based screening using a DSF assay. This assay measures binding of molecules to proteins by changes of the thermal melting profile in the presence of the fluorescent dye Sypro Orange [31]. We validated this assay by testing binding to previously characterized ligands that influence the conformation of Cag α , such as MgCl₂, ADP and the non-hydrolysable substrate analog ATP- γ -S. Addition of the nucleotide ligand MgCl₂ increases the melting temperature from 37°C to 42°C, but in the presence of MgCl₂ and ADP or ATP- γ -S, strong increases of the melting temperature to 55°C and 60°C were observed, respectively (Fig. 1). The optimized assay conditions were used to screen a library of 505 fragments [24, 32] (supplementary Fig. 1) and 16 molecules (supplementary Fig. 2) were identified that reproducibly increase the melting temperature of Cag α by 1°C to 4°C, which is the typical range observed for binding fragments (supplementary Fig. 1). Interestingly, incubation of many of these fragments in the presence of MgCl₂ and ADP reduces the melting temperature when compared to MgCl₂ and ADP alone, suggesting that they impact the conformation of Cag α in a way that changes binding of the other ligands (supplementary Fig. 2).

Effects of binding fragments on the Cag α ATPase activity

We used a Malachite green assay to measure the release of inorganic phosphate from ATP to assess whether the 16 binding fragments impact the enzymatic activity of Cag α . Four of the molecules reduce the ATPase activity and the IC₅₀ values range between 196 μ M for molecule 1G2 and 4.77 mM

in case of molecule 2A5 (Table 1 and supplementary Fig. 4). We used the most potent molecule 1G2 as starting point for a limited structure-activity relationship analysis using six commercially available analogs (Table 2). Two of these molecules (1G2#5 and 1G2#6) do not inhibit the ATPase activity, three of them have higher IC_{50} values than 1G2 (1G2#1, #2 and #3), but molecule 1G2#4 has a lower IC_{50} value of 81.9 μ M (Table 2 and supplementary Fig. 5). Finally, we tested the mechanism of inhibition by varying the inhibitor concentrations (0 to 500 μ M) and the ATP concentrations (0 to 80 μ M) and fitting of the initial velocity data using nonlinear regression shows that only the V_{max} was affected, whereas the K_m -values remain constant (Fig. 2). These results suggest that both molecules are non-competitive inhibitors of Cag α .

Binding fragments impact the conformation and dissociate the Cag α hexamer

Binding of fragments may impact the conformation and the homo-multimerization of Cag α and we used the homo-bifunctional cross-linking agent disuccinimidyl-suberate (DSS) to obtain insights into the multimerization of the protein. As expected, incubation of Cag α with increasing concentrations of DSS (0-20 μ M), followed by SDS-PAGE and western blot analysis, leads to the successive formation of higher molecular mass forms, which is consistent with the formation of a hexamer (Fig. 3a). The cross-linking pattern is similar in the presence of $MgCl_2$ (Fig. 3b), ADP/ $MgCl_2$ (Fig. 3c), and ATP- γ -S/ $MgCl_2$ (Fig. 3d), but in the presence of molecule 1G2 (Fig. 3e) a reduced amount of higher molecular mass complexes is observed suggesting significant changes of the conformation and/or multimerization.

To directly address this question, we performed analytical gel filtration. Purified Cag α elutes in a single peak with an elution volume corresponding to a molecular mass of 244 kDa, which is

consistent with the formation of a hexamer (Fig. 4). The same elution volume was observed in the presence of ATP- γ -S, but interestingly, when Cag α was pre-incubated with molecule 1G2 we observe the elution of two peaks (peak A and peak B in Fig. 4) with elution volumes corresponding to apparent molecular masses of 175 kDa and 54 kDa, respectively. These results suggest that incubation with molecule 1G2 dissociates the Cag α hexamer into lower molecular mass species. Analysis by negative staining electron microscopy reveals hexamers in the absence of 1G2 (Fig. 5a), lower molecule mass species in peak A (Fig. 5b) and even smaller species in peak B (Fig. 5c) confirming this interpretation.

X-ray analysis reveals the 1G2 binding site and conformational changes

To gain further insights into the mechanism of inhibition, we solved the X-ray structure of the Cag α -1G2 complex in the P6322 space group with two molecules in the asymmetric unit (Fig. 6a) to a resolution of 2.9 Å (Table 3). The structure was solved by molecular replacement using ADP bound Cag α (PDB code: 1G6O) as a search model. The overall structure of 1G2-bound Cag α is similar to that of the Cag α -ADP complex, but there are differences of interactions at the protein interface and we identified the electron density of molecule 1G2 sandwiched between two Cag α molecules (Fig. 6a). The monomer structure of the Cag α -1G2 complex displays both NTD and CTD with nine α -helices labeled as α 1 to α 9 and 13 β -strands labeled as β 1 to β 13 (Fig. 6b). A structural overview from the top of the NTD reveals that 1G2 interacts with the NTD of both protein subunits (Fig. 6c). The 1G2 binding site is distinct from the active site to which ADP and the substrate analog ATP- γ -S bind [16, 17]. Molecule 1G2 binds to a hydrophobic pocket created by the interaction between the NTDs of two Cag α subunits and amino acids F68 and F39 make hydrophobic contacts with the two phenyl rings of the inhibitor. R73 and D69 are the amino acids involved in forming a polar contact with 1G2. R73 interacts with the pyridine group of the second phenyl ring via a hydrogen bond and the carboxylic

group of 1G2 interacts with the backbone NH group of D69 forming a potential hydrogen bond (Fig. 6d). Structural alignment of the Cag α -1G2 complex with Cag α -ADP (PDB code: 1G6O) shows an overall similar structure (RMSD 0.6 Å), but we observe shifts of the β 6 and β 7 sheets and in the linker region between NTD and CTD (supplementary Fig. 6). Alignment of Cag α -1G2 with Cag α apoprotein (PDB code: 1NLZ) reveals slight conformational differences in both the CTD and NTD (RMSD 0.9 Å). The α 8 and α 9 helical region of the CTD as well as the α 1 region of the NTD display changes showing that binding to molecule 1G2 impacts the conformation of the protein (supplementary Fig. 6).

Molecule 1G2 inhibits the production of interleukin-8 upon binding of *H. pylori* to AGS cells

Finally, we assessed whether molecule 1G2 or its derivatives impact the functionality of the T4SS *in vivo*. To this effect, we tested their impact on the interaction of *H. pylori* strain 26695 with gastric adenocarcinoma (AGS) cells. First, we tested their toxicity and found that molecule 1G2 and derivatives 1G2#1 to #6 have no negative effect on the growth of *H. pylori* on solid agar media at concentrations up to 500 μ M (supplementary Fig. 7). Similarly, most molecules do not have negative impact on the viability of AGS cells at concentrations up to 500 μ M, showing that they are not toxic (supplementary Fig. 8). When we tested the effects of these molecules at 200 μ M concentration on the production of IL-8 produced by AGS cells upon co-cultivation with *H. pylori*, 1G2 significantly reduces the production of this proinflammatory cytokinin to about 50% of the control (Fig. 7). In contrast, derivatives 1G2#1 to #6 have no effect on IL-8 production and none of the molecules reduces the tyrosine phosphorylation of translocated CagA, which is generally used as an alternative assay to measure T4SS function (supplementary Fig. 9).

Discussion

The fragment-based screening strategy presented here was developed to identify inhibitors of protein-protein interactions and it is generally applicable to bacterial virulence factors for which structural information is available. We have previously used this approach to identify inhibitors of the VirB8 homolog TraE from the plasmid pKM101 conjugation system. We identified molecules that target a known inhibitor binding site on VirB8-like proteins, and we also identified a new binding site showing the potential for the discovery of bioactive molecules and of novel inhibitor target sites [23, 24, 33]. We here used a similar unbiased DSF-based screen to identify fragments that bind Cag α without specifically targeting its ATPase active site. Competitive inhibitors of Cag α ATPase activity are already available [29, 30], and whereas these molecules may have potential for development into anti-virulence drugs, the possibility that they bind other ATPases in bacteria or in host cells remains a concern.

We here identified molecules that inhibit the Cag α ATPase activity indirectly via a novel allosteric mechanism. Enzyme kinetic analyses showed that the mechanism of inhibition by molecules 1G2 and 1G2#4 is non-competitive. Analysis of the X-ray structure showed that molecule 1G2 binds at the interface between Cag α molecules that multimerize via the NTD and this is consistent with the results of enzyme kinetics. The non-competitive mechanism of inhibition is similar to that reported in the case of unsaturated 2-alkynoic fatty acids that inhibit the VirB11 homolog TrwD from plasmid R388 [27, 28]. Docking predicted a potential binding site for these molecules at the linker region between the NTD and the CTD of a structural model of TrwD. However, high-resolution structural information on TrwD and on the potential binding site is not available and this site is distinct from the 1G2 binding site we observe by X-ray crystallography. Analysis of the Cag α -1G2 X-ray structure

revealed subtle conformational changes in different parts of the protein including the active site as compared to the apoprotein and its complex with ADP. This may explain the effect of 1G2 binding on the enzymatic activity of Cag α . Conformational changes were also observed by cross-linking and comparable observations were made in the case of TrwD that became more susceptible to protease degradation in the presence of 2-alkynoic fatty acids [27]. Intriguingly, gel filtration and EM analysis revealed that binding to 1G2 successively dissociates the Cag α -hexamer. This mechanism is entirely novel and it would be interesting to assess the molecular basis of dissociation using approaches that are more sensitive to conformational changes than X-ray crystallography, such as cryo-electron microscopy. Also, in the context of the current work we have not assessed the potential of most of the other Cag α -binding molecules that do not inhibit the ATPase activity. These molecules may bind different sites of the protein and may have interesting biological activity that remains to be explored in future.

Cag α is essential for type IV secretion and deletion of the encoding gene inhibits IL8 production and CagA transfer into AGS cells, which are the most commonly used readouts for *H. pylori* T4SS function [9, 10]. The results for IL-8 production and CagA phosphorylation usually correlate when the effects of *cag* gene mutations are determined. It was therefore somewhat unexpected that molecule 1G2 inhibited IL-8 production to 50% of the control values, but we did not observe an effect on CagA phosphorylation. This observation may be due to the partial inhibition of T4SS function by 1G2 that is more readily quantifiable in the IL-8 production assay as compared to the CagA phosphorylation assay. Enzyme kinetic analysis showed that molecule 1G2#4 was significantly more potent than 1G2 *in vitro*, but repeated crystallisation trials of Cag α with 1G2#4 were unsuccessful. Soaking of 1G2#4 into Cag α crystals resulted in crystal cracking, suggesting a conformational change in Cag α and/or dissociation of the Cag α quaternary structure. This may be due to the higher potency of

molecule 1G2#4 that could be explained by additional hydrophobic contacts of its additional methyl group with amino acid K41 (supplementary Fig. 10). However, this molecule had no effect in the *in vivo* assays, which may be due to its higher hydrophobicity impacting solubility and penetration into cells.

We have here analyzed six derivatives of molecule 1G2 that were commercially available and in future work we will conduct a structure-based structure-activity relationship analysis to synthesize more potent molecules that efficiently penetrate into cells. This approach will enable us to assess whether inhibition of Cag α leads to differential effects on the translocation of effectors CagA, HBP and murein that might also explain the differential effect of molecule 1G2 on IL-8 production and CagA phosphorylation. Potent inhibitors of Cag α could be developed into anti-virulence drugs that are alternative or complementary treatments to currently used triple or quadruple therapy. It would also be interesting to test the specificity of these molecules to assess whether they are narrow or broad spectrum inhibitors that also impact other T4SS, e.g. bacterial conjugation systems [28, 34].

Methods

Bacterial strains, cell lines and culture conditions.

H. pylori strains 26695 and Δ cagV (*hp0530*) mutant have been described [35] and were cultivated on Columbia agar base (BD) containing 10% (v/v) defibrinated horse blood (Winsent Inc.), vancomycin (10 µg/L) and amphotericin B (10 µg/L). Chloramphenicol (34 µg/L) was added in case of the Δ cagV strain to select for the cam gene cassette used to disrupt the gene. For liquid culture, brain heart infusion (BHI) media (Oxoid) were supplemented with 8% fetal bovine serum (FBS) and appropriate antibiotics. Bacteria were cultivated at 37°C, under microaerophilic conditions (5% oxygen, 10% CO₂). AGS cells were grown at 37°C in F12K media (Winsent Inc.) with 10% (v/v) FBS (Winsent Inc.) in a 5% CO₂ containing atmosphere.

Cloning, expression and purification of Cagα

The Cagα encoding gene from *H. pylori* 26695 (ATTC) was PCR-amplified from genomic DNA with primers (forward, 5'-TAGCGAATTCGGTACCATGACTGAAGACAGATTGAGTGCA-3' and reverse, 5'-CGATGAATTCCTCGAGCTACCTGTGTGTTTGATATAAAATTC-3'), thereby adding an N-terminal hexahistidyl-tag and a TEV cleavage site, and the PCR product was cleaved with restriction enzymes *NheI* and *XhoI*, followed by ligation into expression vector pET28a. Expression was conducted in *E. coli* BL21 (DE3) cultivated in two liters of LB-medium at 37 °C at 220 rpm, protein production was induced at OD₆₀₀ of 1 with 1 mM isopropylthio-β-galactoside (IPTG), followed by further incubation for 16h at 25°C. For purification, the cell pellet was suspended in binding buffer (50 mM HEPES, 500 mM NaCl, 20 mM imidazole, pH 7.5, 10% glycerol, 0.1% triton, plus two tablets

of EDTA-free protease inhibitor cocktail (Roche)) and lysed using a cell disrupter (Constant Systems Inc.) at 27 kPsi, followed by centrifugation at 15,000 rpm at 4°C to reduce cell debris. The supernatant was loaded onto a His-trap Ni-NTA column (GE Healthcare), which was pre-equilibrated with 100 ml of binding buffer. Then protein was eluted using a linear 50 ml gradient of 40-500 mM imidazole in binding buffer. Proteins were then desalted into TEV buffer (25 mM sodium phosphate, 125 mM NaCl, 5 mM DTT, pH 7.4) and subjected to cleavage of the N-terminal 6x-His-tag using TEV protease in a ratio of 1:70 (TEV:protein) for 24 h at 20°C. The cleaved protein was dialysed into 50 mM HEPES, 100 mM pH 7.5 buffer and concentrated with Amicon filters. Size exclusion chromatography was conducted using a Superdex-200 column (GE Healthcare) with buffer 25 mM HEPES pH7.5 and 100 mM NaCl and peak fractions were analyzed by SDS-PAGE. The fractions containing Cag α hexamers were pooled and concentrated to 6 mg/ml for crystallographic studies.

Analytical gel filtration chromatography

Purified protein was further characterized by analytical gel filtration (Superdex 200) in 25 mM HEPES, pH 7.5 and 50 mM NaCl (pH 7.5). The column volume was 3ml and the protein was injected at a flow rate of 0.5 ml/min. To study the effects of ATP- γ -S and of 1G2, 35 μ g of Cag α was pre-incubated with 2 mM of the molecules for 30 min, followed by analytical size exclusion analysis.

Enzyme activity assay

The ATPase activity was quantified using a malachite green binding assay [36]. The 100 μ L reaction mixtures contained 25 mM HEPES (pH 7.5), 100 mM NaCl, 60 nM of enzyme and 200 μ M of MgCl₂ with different concentrations of ATP (0 μ M – 320 μ M) to determine kinetic parameters. The

reaction mixtures were incubated for 30 min at 30°C and then 40 µL of malachite green assay mixture was added. The formation of the blue phosphomolybdate-malachite green complex was in linear relation to the amount of released inorganic phosphate and measured at 610 nm. To study the mechanism of inhibition, the concentrations of inhibitors were varied between 0 and 500 µM with different concentrations of ATP (0-40 µM). Initial velocity data were fit using nonlinear regression analysis to each of the equations describing partial and full models of competitive, uncompetitive, non-competitive, and mixed inhibition using the Enzyme Kinetics Module of SigmaPlot (SigmaPlot version 11.0 software). On the basis of the analysis of fits through “goodness-of-fit” statistics, the full non-competitive inhibition model was determined with the equation $v = V_{\max}/[(1 + [I]/K_i) \times (1 + K_m/[S])]$, where $[S] = [ATP]$, $[I] = [1G2]$.

IC₅₀ determination

IC₅₀ values were determined by incubating different concentrations of molecules (10 - 1,000 µM; from stocks of 200 mM) with enzyme in 25 mM HEPES (pH 7.5) and 100 mM NaCl. Mixtures were incubated with inhibitors for 15 min, followed by addition of ATP and incubation for 30 min at 37 °C. The reactions were stopped by addition of 40 µl malachite green solution and the inorganic phosphate released was determined at 610 nm. Data were plotted as 1/rate versus inhibitor concentration for each substrate concentration and a linear fit was calculated by non-linear regression using SigmaPlot (version 11.0).

Differential scanning fluorimetry (DSF)

A fragment library of 505 molecules was used as in our previous work [32]. The reaction mixture contains 5 µM of Cagα, 10x concentration of SYPRO Orange (from 5000x stock solution

(ThermoFisher)) in 50 mM HEPES (pH 7.5), 100 mM NaCl and 5% final concentration of DMSO. The fragments and nucleotides were added to final concentrations of 5 mM, and the fluorescence was monitored over 20–95 °C with a LightCycler 480 instrument (Roche).

Crystallisation and structure determination

Initial crystallization conditions were established using the MCSG screen from (ANATRACE, USA) using 6 mg/ml of Cag α and 1 mM of 1G2 (1:10 ratio). Final crystals were grown at room temperature using the hanging drop vapour diffusion method in 100 mM Bis-Tris (pH 6.5) and 2 M ammonium sulfate. Drops containing 2 μ l of protein-inhibitor-mixture (1:10 ratio) and 2 μ l of reservoir solution were incubated for 2 weeks. Hexagonally-shaped crystals appeared after 7-10 days. The crystals were cryo-protected in 100 mM Tris-HCl buffer (pH 8.5), 2 M ammonium sulfate and 25% glycerol, flash frozen in liquid nitrogen and the data were collected at microfocus beamline F1 at the Cornell High Energy Synchrotron Source (CHESS). The intensity data was processed using the HKL2000 [37] program in p6522 space group (Table 3) . The structure was solved by molecular replacement using the coordinates of PDB ID: 1G6O as search model. Refinement and modeling were performed using REFMAC and Coot [38, 39]. Final graphical figures and tables were generated using the Pymol-integrated Phenix software suite [40].

Analysis of protein-protein interactions by cross-linking

Chemical cross-linking with disuccinimidyl suberate (DSS; Pierce) was performed as described [41]. 100 nM of Cag α in 50 mM HEPES (pH 7.5) and 100 mM NaCl were first incubated with cofactors (MgCl₂, ADP) or inhibitors (ATP- γ -S, 1G2) for 30 min, followed by crosslinking with DSS (0

- 50 μ M) for 1 h, and reactions were stopped by mixing with an equal volume of 2 x Laemmli buffer. The formation of cross-linking products was analyzed by SDS-PAGE and western blotting using His-tag specific antiserum and ImageLab 4.0 software (Bio-Rad)

Electron microscopy and image processing

Carbon-coated grids were negatively glow-discharged at 15 mA and 0.4 mBar for 30 sec. 5 μ l of purified protein at a concentration of 2 ng/ μ l was spotted onto the grids for 60 sec and blotted using grade 1 Whatman filter paper, followed by staining with freshly prepared 1.5% uranyl formate solution for 60 sec and drying. The samples were imaged at a magnification of 49,000-fold (pixel size: 2.2 Å/pixel) with a defocus of -2.5 μ m using a FEI Tecnai T12 electron microscope (FEMR facility at McGill University). Transmission Electron Microscope (TEM) equipped with a Tungsten filament and operated at 120 kV equipped with a 4k x 4k CCD camera (Gatan Ultrascan 4000 CCD camera system model 895). Subsequently, the images were processed using ImageJ.

Measurement of *H. pylori* and AGS cell viability

AGS cell viability was monitored using Cell Proliferation Reagent WST-1 (Sigma). To evaluate the sensitivity of *H. pylori* to 1G2 and its derivatives, freshly harvested bacteria were spread on a 150-mm agar plate. Increasing concentrations of compounds (50-500 μ M) were spotted onto Whatman paper disks and growth was observed after 72h incubation at 37°C under microaerophilic conditions and compared to antibiotics (50-250 μ M).

Assay for monitoring CagA transfer into AGS cells

Preceding the infection, an overnight culture of *H. pylori* was pre-incubated with 1G2 and its derivatives for 30 min. AGS cells at 6×10^5 cells/well density in 6-well plates were infected with the pre-treated cultures of *H. pylori* for 3-6 h at a multiplicity of infection of 100:1. Cells were washed twice with PBS, harvested and lysed at 4°C in RIPA buffer (150 mM NaCl, 50 mM Tris/ HCl, pH 8, 1% NP-40, 2 mM Na_3VO_4 , supplemented with Complete Protease Inhibitor Tablet (Roche). After 15 min of centrifugation at 16,000 g, lysates were separated by SDS-PAGE, followed by western blotting with mouse polyclonal antiserum raised against CagA (Abcam), anti-phosphotyrosine (PY99; Santa Cruz Biotechnology) and anti- β -actin (C4, Santa Cruz Biotechnology).

Assay for IL-8 induction

Preceding the infection, an overnight culture of *H. pylori* was pre-incubated with 1G2 and its derivatives for 30 min. AGS cells at 6×10^5 cells/well density in 6-well plates were infected with the pre-treated cultures of *H. pylori* at a multiplicity of infection of 100:1. After 24 h incubation under microaerophilic conditions, supernatants were sampled and centrifuged (15,000 g), before freezing at -80°C. The level of IL-8 in cell culture supernatants was determined by using a commercially available human IL-8 ELISA kit (Invitrogen).

Acknowledgements

This work was supported by grants to C.B. from the Canadian Institutes of Health Research (CIHR MOP-84239)(<http://www.cihr-irsc.gc.ca/>), the NSERC-CREATE program on the Cellular Dynamics of Macromolecular Complexes (CDMC) (<http://www.nserc-crsng.gc.ca/>), a seed grant from Merck, Sharp and Dohme (<http://www.merck.ca/>), the Canada Foundation for Innovation (CFI)(<https://www.innovation.ca/>) and the Fonds de recherche du Québec-Santé (FRQ-S)(<http://www.frqs.gouv.qc.ca/>). We are grateful to Edward Ruediger and his colleagues at the medicinal chemistry platform at IRIC (Institut de recherche en immunologie et en oncologie (IRIC), Université de Montréal) for support with small molecule screening. We thank Dr. Aleksandr Sverzhinsky from the Department of Biochemistry and Molecular Medicine for helping us with analytical chromatography. We are thankful to Dr. Martin Schmeing and Dr. Asfarul Haque (Department of Biochemistry, McGill University) for helping us with data collection at the Facility of Electron Microscopy Research (FEMR) at McGill University. Synchrotron X-ray data were collected at the Cornell High Energy Synchrotron Source (CHESS, MacCHESS beamline F1).

Tables

Table 1: Structures and IC₅₀ of molecules that inhibit the ATPase activity of Cagα.

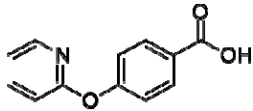
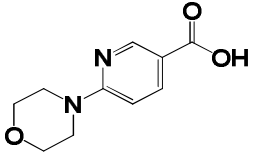
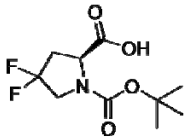
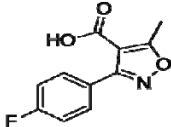
Name	Structure	IC ₅₀ values (μM)
1G2		196.2 (± 0.026) μM
1G6		0.987 (±0.076) mM
2A5		4.77 (±0.053) mM
1F12		1.85(± 0.068) mM

Table 2: Structures of derivates of molecules 1G2 and their effects on the ATPase activity of Cagα.

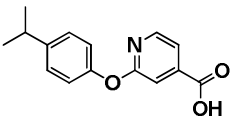
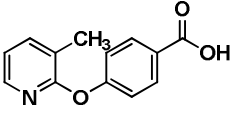
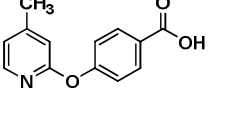
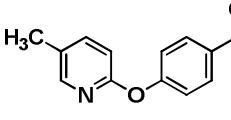
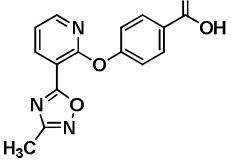
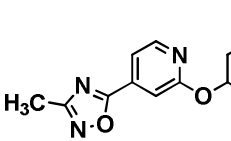
Name	Structure	IC ₅₀ values (μM)
1G2#1		547.4 (±0.59)
1G2#2		619.6 (±0.95)
1G2#3		479.6 (±0.46)
1G2#4		81.9 (±0.6)
1G2#5		No Inhibition
1G2#6		No Inhibition

Table 3: Data collection and refinement statistics.

	Cagα-1G2
Resolution range	38.48 - 2.802 (2.902 - 2.802)
Space group	P 63 2 2
Unit cell	112.092 112.092 230.889 90 90 120
Total reflections	197211
Unique reflections	19828 (1836)
Multiplicity	10.1
Completeness (%)	90.44 (87.30)
Mean I/sigma(I)	2.33
Wilson B-factor	44.26
R-merge	0.10
R-pim	0.08
Reflections used in refinement	19787 (1835)
Reflections used for R-free	976 (92)
R-work	0.2570 (0.3280)
R-free	0.3266 (0.3991)
Protein residues	646
RMS(bonds)	0.013
RMS(angles)	1.62
Ramachandran favored (%)	93.15
Ramachandran allowed (%)	5.30

Ramachandran outliers (%)	1.56
Rotamer outliers (%)	6.50
Clashscore	3.87
Average B-factor	46.27
PDB	6BGE

Legends to the figures

Figure 1. Melting temperature of Cag α in the presence of ligands and cofactors. Melting curves for Cag α were determined using differential scanning fluorimetry (DSF). (A) Cag α apoprotein (green), (B) Cag α and metal cofactor MgCl₂ (pink), (C) Cag α with ADP (blue) and (D) Cag α with ATP- γ -S (black). Table in the upper right corner shows melting temperatures.

Figure 2. Enzyme Kinetics of Cag α in the presence of molecule 1G2 and 1G2#4. (a, c) Dose response curves of ATPase activity showing IC₅₀ values in the presence of 1G2 and its derivative 1G2#4. (b, d) Lineweaver-Burke plot of Cag α ATPase activity in the presence of 1G2 and 1G2#4. The data were globally fit to a model of non-competitive inhibition. Concentrations varied from 0 to 500 μ M of inhibitors in the presence of 2 mM of MgCl₂.

Figure 3. Chemical cross-linking using DSS to study the formation of Cag α oligomers in the presence of ligands. a) Cag α apo protein; b) Cag α with MgCl₂; c) Cag α with ADP and MgCl₂; d) Cag α with ATP- γ -S and MgCl₂; e) Cag α with 1G2 and MgCl₂. The concentrations of DSS varied between 0 and 50 μ M leading to formation of oligomers (indicated by arrows), detection by SDS-PAGE and western blotting using His-tag specific antibodies.

Figure 4. Analytical size exclusion chromatography of Cag α apoprotein and in the presence of ligands. Proteins were separated by gel filtration over a Superdex 200 column. Cag α apoprotein elutes as a hexamer (red curve), elution of Cag α -ATP- γ -S (blue curve) and of two lower molecular mass peaks (A and B) after incubation of Cag α with 1G2 (in green). The molecular masses characterized according to the elution volume are summarized in the table above the graph.

Figure 5. Electron micrographs of negatively stained Cag α apoprotein after gel filtration.

Analysis by transmission electron microscopy and negative staining of a) Cag α apoprotein shows a hexameric ring-like structure; b) peak A of Cag α incubated with 1G2 after elution from the gel-filtration and c) peak B. d) negative control grid. Arrows show the differently sized complexes.

Figure 6. Crystal structure of the Cag α bound to molecule 1G2.

a) Cartoon representation of the crystal structure of Cag α crystallized as two molecules in the asymmetric unit. Red map in middle of two subunits represents molecule 1G2. b) Representation of the monomeric subunit of Cag α in ribbon form: α helices, β strands and loops are represented in yellow, red and green, respectively. The nine helices are labeled as α 1 to α 9 and the β -strands are labeled as β 1 to β 13. c) Side view of the interaction of two subunits of protein with 1G2 in the middle represented as green stick and red map. d) Enlarged view of 1G2 binding at the interface between two protein subunits. The $2F_o - F_c$ electron density map of 1G2 was contoured at 1.5σ .

Figure 7. Molecule 1G2 decreases IL-8 induction in co-cultivated AGS cells.

H. pylori 26695 without and after pre-incubation with 1G2 and its derivatives for 40 min. AGS cells were then co-cultured with *H. pylori* overnight and IL-8 induction was measured by ELISA. The induction of IL-8 by the wild type was calculated as 100% (WT), induction of IL-8 by the Δ cagV strain was used as negative control. The data represent the results from three experiments.

References

1. Malfertheiner P, Link A, Selgrad M. Helicobacter pylori: perspectives and time trends. Nature reviews Gastroenterology & hepatology. 2014;11(10):628-38. doi: 10.1038/nrgastro.2014.99. PubMed PMID: 25001975.
2. Herrero R, Parsonnet J, Greenberg ER. Prevention of gastric cancer. Jama. 2014;312(12):1197-8. doi: 10.1001/jama.2014.10498. PubMed PMID: 25247512.
3. Plummer M, Franceschi S, Vignat J, Forman D, de Martel C. Global burden of gastric cancer attributable to Helicobacter pylori. International journal of cancer Journal international du cancer. 2015;136(2):487-90. doi: 10.1002/ijc.28999. PubMed PMID: 24889903.
4. Gatta L, Vakil N, Vaira D, Scarpignato C. Global eradication rates for Helicobacter pylori infection: systematic review and meta-analysis of sequential therapy. Bmj. 2013;347:f4587. doi: 10.1136/bmj.f4587. PubMed PMID: 23926315; PubMed Central PMCID: PMC3736972.
5. Ochman H, Lawrence JG, Groisman EA. Lateral gene transfer and the nature of bacterial innovation. Nature. 2000;405(6784):299-304. Epub 2000/06/01. doi: 10.1038/35012500. PubMed PMID: 10830951.
6. Grohmann E, Christie PJ, Waksman G, Backert S. Type IV secretion in Gram-negative and Gram-positive bacteria. Molecular microbiology. 2018;107(4):455-71. Epub 2017/12/14. doi: 10.1111/mmi.13896. PubMed PMID: 29235173; PubMed Central PMCID: PMC5796862.
7. Segal ED, Cha J, Lo J, Falkow S, Tompkins LS. Altered states: involvement of phosphorylated CagA in the induction of host cellular growth changes by Helicobacter pylori. Proc Natl Acad Sci U S A. 1999;96(25):14559-64. Epub 1999/12/10. PubMed PMID: 10588744; PubMed Central PMCID: PMC24475.

8. Backert S, Ziska E, Brinkmann V, Zimny-Arndt U, Fauconnier A, Jungblut PR, et al. Translocation of the *Helicobacter pylori* CagA protein in gastric epithelial cells by a type IV secretion apparatus. *Cellular microbiology*. 2000;2(2):155-64. Epub 2001/02/24. PubMed PMID: 11207572.
9. Fischer W, Püls J, Buhrdorf R, Gebert B, Odenbreit S, Haas R. Systematic mutagenesis of the *Helicobacter pylori* *cag* pathogenicity island: essential genes for CagA translocation in host cells and induction of interleukin-8. *Mol Microbiol*. 2001;42:1337-48.
10. Selbach M, Moese S, Meyer TF, Backert S. Functional analysis of the *Helicobacter pylori* *cag* pathogenicity island reveals both VirD4-CagA-dependent and VirD4-CagA-independent mechanisms. *Infect Immun*. 2002;70:665-71.
11. Tegtmeyer N, Neddermann M, Asche CI, Backert S. Subversion of host kinases: a key network in cellular signaling hijacked by *Helicobacter pylori* CagA. *Molecular microbiology*. 2017;105(3):358-72. Epub 2017/05/17. doi: 10.1111/mmi.13707. PubMed PMID: 28508421.
12. Naumann M, Sokolova O, Tegtmeyer N, Backert S. *Helicobacter pylori*: A Paradigm Pathogen for Subverting Host Cell Signal Transmission. *Trends Microbiol*. 2017;25(4):316-28. Epub 2017/01/07. doi: 10.1016/j.tim.2016.12.004. PubMed PMID: 28057411.
13. Gall A, Gaudet RG, Gray-Owen SD, Salama NR. TIFA Signaling in Gastric Epithelial Cells Initiates the *cag* Type 4 Secretion System-Dependent Innate Immune Response to *Helicobacter pylori* Infection. *MBio*. 2017;8(4). Epub 2017/08/16. doi: 10.1128/mBio.01168-17. PubMed PMID: 28811347; PubMed Central PMCID: PMC5559637.
14. Krause S, Barcena M, Pansegrau W, Lurz R, Carazo JM, Lanka E. Sequence-related protein export NTPases encoded by the conjugative transfer region of RP4 and by the *cag* pathogenicity island of *Helicobacter pylori* share similar hexameric ring structures. *Proc Natl Acad Sci U S A*. 2000;97(7):3067-72. Epub 2000/03/15. doi: 10.1073/pnas.050578697050578697 [pii]. PubMed PMID: 10716714; PubMed Central PMCID: PMC16193.

15. Krause S, Pansegrau W, Lurz R, de la Cruz F, Lanka E. Enzymology of type IV macromolecule secretion systems: the conjugative transfer regions of plasmids RP4 and R388 and the cag pathogenicity island of *Helicobacter pylori* encode structurally and functionally related nucleoside triphosphate hydrolases. *J Bacteriol.* 2000;182(10):2761-70. Epub 2000/04/27. PubMed PMID: 10781544; PubMed Central PMCID: PMC101984.
16. Savvides SN, Yeo HJ, Beck MR, Blaesing F, Lurz R, Lanka E, et al. VirB11 ATPases are dynamic hexameric assemblies: new insights into bacterial type IV secretion. *EMBO J.* 2003;22:1969-80.
17. Yeo HJ, Savvides SN, Herr AB, Lanka E, Waksman G. Crystal structure of the hexameric traffic ATPase of the *Helicobacter pylori* type IV secretion system. *Mol Cell.* 2000;6:1461-72.
18. Fujita Y, Krause G, Scheffner M, Zechner D, Leddy HE, Behrens J, et al. Hakai, a c-Cbl-like protein, ubiquitinates and induces endocytosis of the E-cadherin complex. *Nat Cell Biol.* 2002;4(3):222-31. PubMed PMID: 11836526.
19. Hare S, Bayliss R, Baron C, Waksman G. A large domain swap in the VirB11 ATPase of *Brucella suis* leaves the hexameric assembly intact. *Journal of molecular biology.* 2006;360(1):56-66. Epub 2006/05/30. doi: S0022-2836(06)00554-7 [pii] 10.1016/j.jmb.2006.04.060. PubMed PMID: 16730027.
20. Brown ED, Wright GD. Antibacterial drug discovery in the resistance era. *Nature.* 2016;529(7586):336-43. doi: 10.1038/nature17042. PubMed PMID: 26791724.
21. Ruer S, Pinotsis N, Steadman D, Waksman G, Remaut H. Virulence-targeted Antibacterials: Concept, Promise, and Susceptibility to Resistance Mechanisms. *Chem Biol Drug Des.* 2015;86(4):379-99. doi: 10.1111/cbdd.12517. PubMed PMID: 25589217.
22. Paschos A, den Hartigh A, Smith MA, Atluri VL, Sivanesan D, Tsolis RM, et al. An In Vivo High-Throughput Screening Approach Targeting the Type IV Secretion System Component VirB8

Identified Inhibitors of *Brucella abortus* 2308 Proliferation. *Infect Immun*. 2011;79(3):1033-43. Epub 2010/12/22. doi: IAI.00993-10 [pii]

10.1128/IAI.00993-10. PubMed PMID: 21173315.

23. Smith MA, Coincon M, Paschos A, Jolicoeur B, Lavallee P, Sygusch J, et al. Identification of the Binding Site of *Brucella* VirB8 Interaction Inhibitors. *Chem Biol*. 2012;19(8):1041-8. Epub 2012/08/28. doi: S1074-5521(12)00230-X [pii]

10.1016/j.chembiol.2012.07.007. PubMed PMID: 22921071.

24. Casu B, Arya T, Bessette B, Baron C. Fragment-based screening identifies novel targets for inhibitors of conjugative transfer of antimicrobial resistance by plasmid pKM101. *Sci Rep*.

2017;7(1):14907. doi: 10.1038/s41598-017-14953-1. PubMed Central PMCID: PMC5668240.

25. Casu B, Smart JP, Hancock MA, Smith M, Sygusch J, Baron C. Structural analysis and inhibition of TraE from the pKM101 type IV secretion system. *J Biol Chem*. 2016;291:23817-29.

26. Shaffer CL, Good JA, Kumar S, Krishnan KS, Gaddy JA, Loh JT, et al. Peptidomimetic Small Molecules Disrupt Type IV Secretion System Activity in Diverse Bacterial Pathogens. *MBio*.

2016;7(2):e00221-16. Epub 2016/04/28. doi: 10.1128/mBio.00221-16

e00221-16 [pii]

mBio.00221-16 [pii]. PubMed PMID: 27118587; PubMed Central PMCID: PMC4850256.

27. Ripoll-Rozada J, Garcia-Cazorla Y, Getino M, Machon C, Sanabria-Rios D, de la Cruz F, et al. Type IV traffic ATPase TrwD as molecular target to inhibit bacterial conjugation. *Molecular microbiology*. 2016;100(5):912-21. Epub 2016/02/27. doi: 10.1111/mmi.13359. PubMed PMID: 26915347; PubMed Central PMCID: PMC4908816.

28. Cabezon E, de la Cruz F, Arechaga I. Conjugation Inhibitors and Their Potential Use to Prevent Dissemination of Antibiotic Resistance Genes in Bacteria. *Front Microbiol*. 2017;8:2329. Epub 2017/12/20. doi: 10.3389/fmicb.2017.02329. PubMed PMID: 29255449; PubMed Central PMCID: PMC5723004.

29. Hilleringmann M, Pansegrau W, Doyle M, Kaufman S, MacKichan ML, Gianfaldoni C, et al. Inhibitors of *Helicobacter pylori* ATPase Cagalpha block CagA transport and cag virulence. *Microbiology*. 2006;152(Pt 10):2919-30. PubMed PMID: 17005973.
30. Sayer JR, Wallden K, Pesnot T, Campbell F, Gane PJ, Simone M, et al. 2- and 3-substituted imidazo[1,2-a]pyrazines as inhibitors of bacterial type IV secretion. *Bioorg Med Chem*. 2014;22(22):6459-70. doi: 10.1016/j.bmc.2014.09.036. PubMed PMID: 25438770; PubMed Central PMCID: PMC4339681.
31. Mashalidis EH, Sledz P, Lang S, Abell C. A three-stage biophysical screening cascade for fragment-based drug discovery. *Nature protocols*. 2013;8(11):2309-24. doi: 10.1038/nprot.2013.130. PubMed PMID: 24157549.
32. Sharifahmadian M, Arya T, Bessette B, Lecoq L, Ruediger E, Omichinski JG, et al. Monomer-to-dimer transition of *Brucella suis* type IV secretion system component VirB8 induces conformational changes. *The FEBS journal*. 2017;284(8):1218-32. doi: 10.1111/febs.14049. PubMed PMID: 28236662.
33. Casu B, Mary C, Sverzhinsky A, Fouillen A, Nanci A, Baron C. The VirB8 homolog TraE from the plasmid pKM101 type IV secretion system interacts with TraD and forms a hexameric ring-like pore structure submitted to PNAS (accepted for review). 2018.
34. Zambelloni R, Marquez R, Roe AJ. Development of antivirulence compounds: a biochemical review. *Chem Biol Drug Des*. 2015;85(1):43-55. doi: 10.1111/cbdd.12430. PubMed PMID: 25521644.
35. Fischer W, Puls J, Buhrdorf R, Gebert B, Odenbreit S, Haas R. Systematic mutagenesis of the *Helicobacter pylori* cag pathogenicity island: essential genes for CagA translocation in host cells and induction of interleukin-8. *Mol Microbiol*. 2001;42(5):1337-48. PubMed PMID: 11886563.
36. Cogan EB, Birrell GB, Griffith OH. A robotics-based automated assay for inorganic and organic phosphates. *Anal Biochem*. 1999;271(1):29-35. Epub 1999/06/11. doi: 10.1006/abio.1999.4100 S0003-2697(99)94100-3 [pii]. PubMed PMID: 10361001.

37. Otwinowski Z, Minor W. Processing of X-ray diffraction data collected in oscillation mode. *Methods Enzymol.* 1997;276:307-26. Epub 1997/01/01. PubMed PMID: 27754618.
38. Murshudov GN, Vagin AA, Dodson EJ. Refinement of macromolecular structures by the maximum-likelihood method. *Acta crystallographica Section D, Biological crystallography.* 1997;53(Pt 3):240-55. doi: 10.1107/S0907444996012255. PubMed PMID: 15299926.
39. Emsley P, Cowtan K. Coot: model-building tools for molecular graphics. *Acta crystallographica Section D, Biological crystallography.* 2004;60(Pt 12 Pt 1):2126-32. Epub 2004/12/02. doi: S0907444904019158 [pii] 10.1107/S0907444904019158. PubMed PMID: 15572765.
40. Adams PD, Grosse-Kunstleve RW, Hung LW, Ioerger TR, McCoy AJ, Moriarty NW, et al. PHENIX: building new software for automated crystallographic structure determination. *Acta crystallographica Section D, Biological crystallography.* 2002;58(Pt 11):1948-54. Epub 2002/10/24. doi: S0907444902016657 [pii]. PubMed PMID: 12393927.
41. Yuan Q, Carle A, Gao C, Sivanesan D, Aly KA, Hoppner C, et al. Identification of the VirB4-VirB8-VirB5-VirB2 pilus assembly sequence of type IV secretion systems. *J Biol Chem.* 2005;280(28):26349-59. Epub 2005/05/20. doi: M502347200 [pii] 10.1074/jbc.M502347200. PubMed PMID: 15901731.

Figure 1

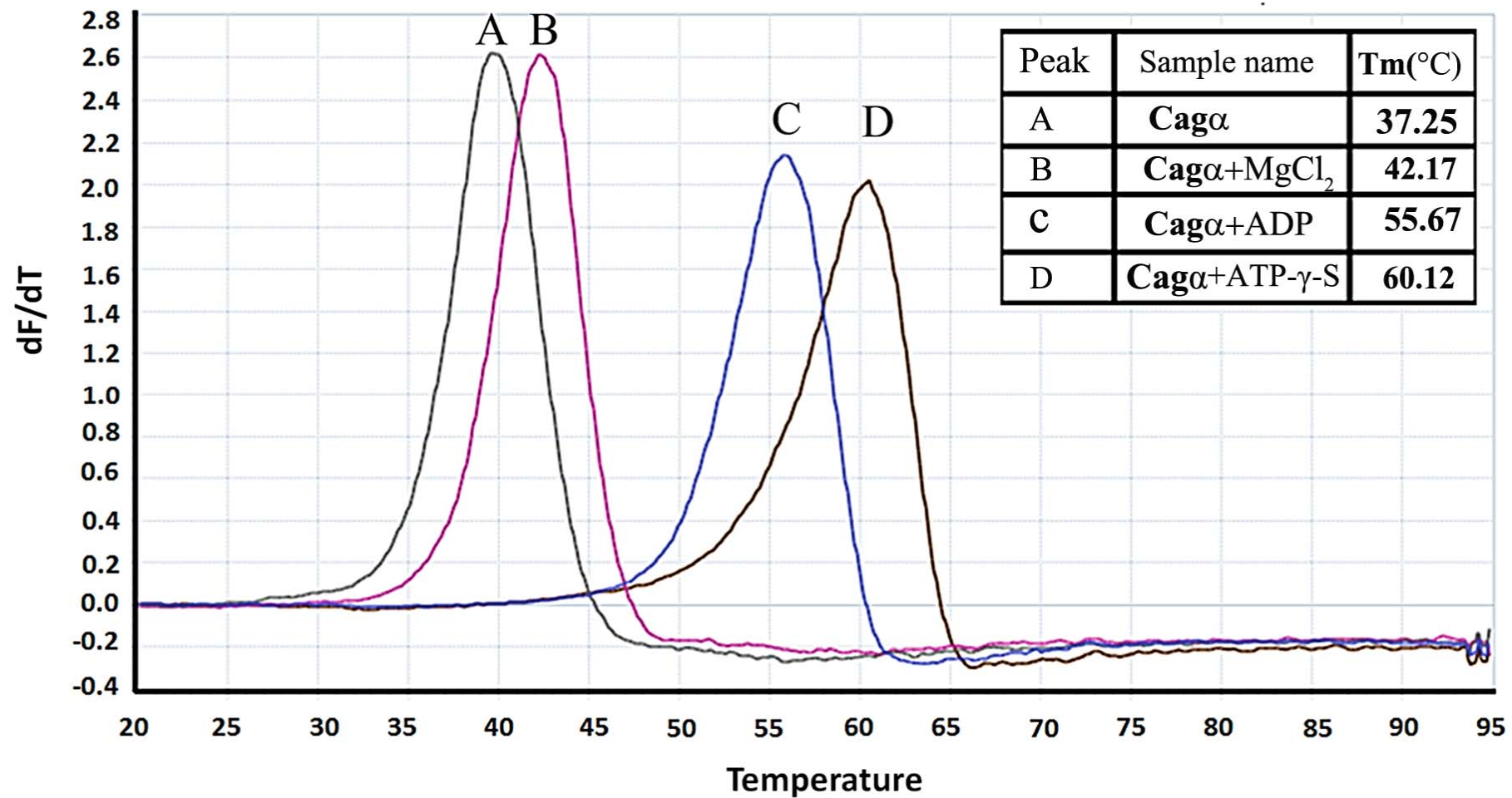


Figure 2

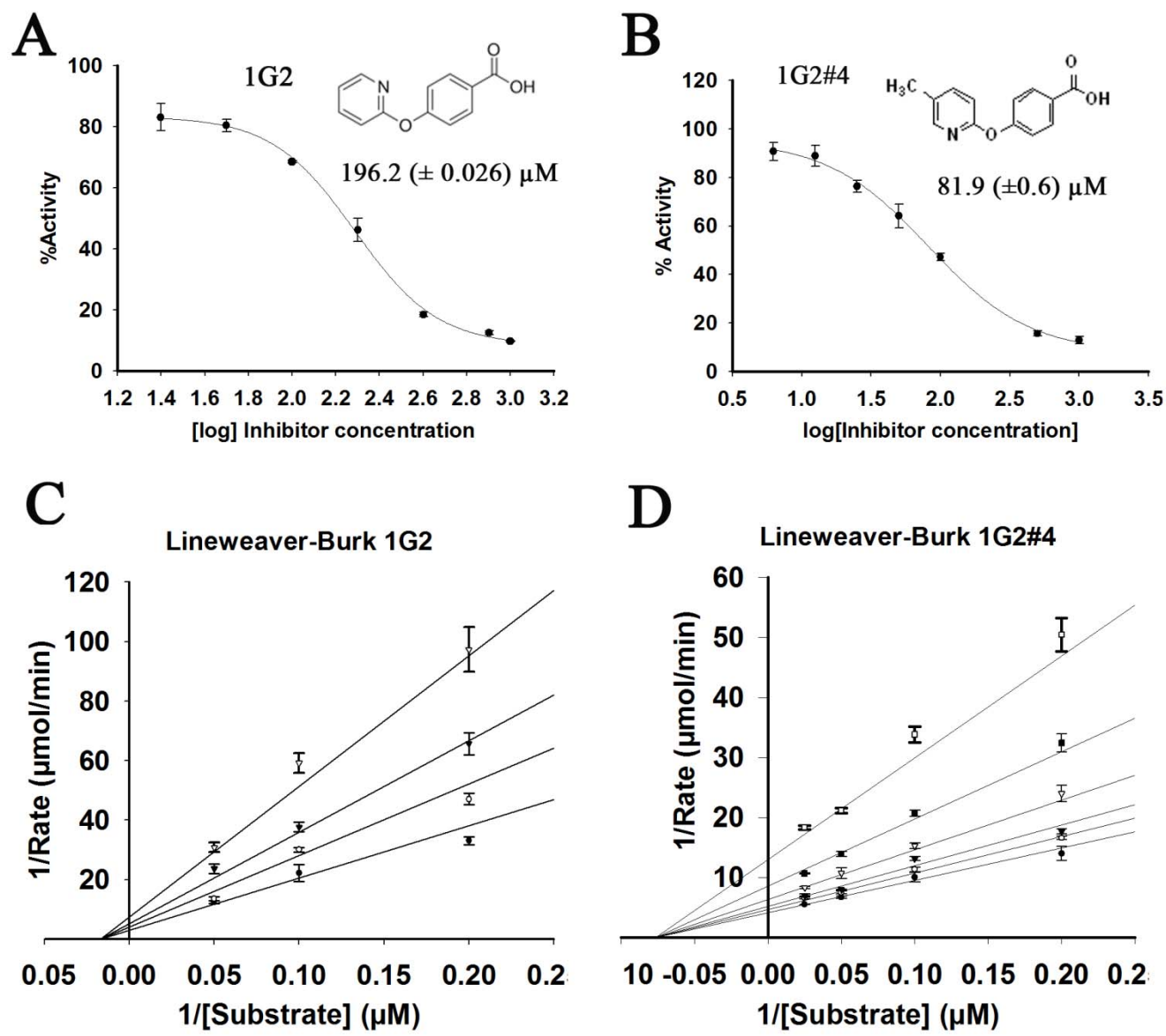


Figure 3

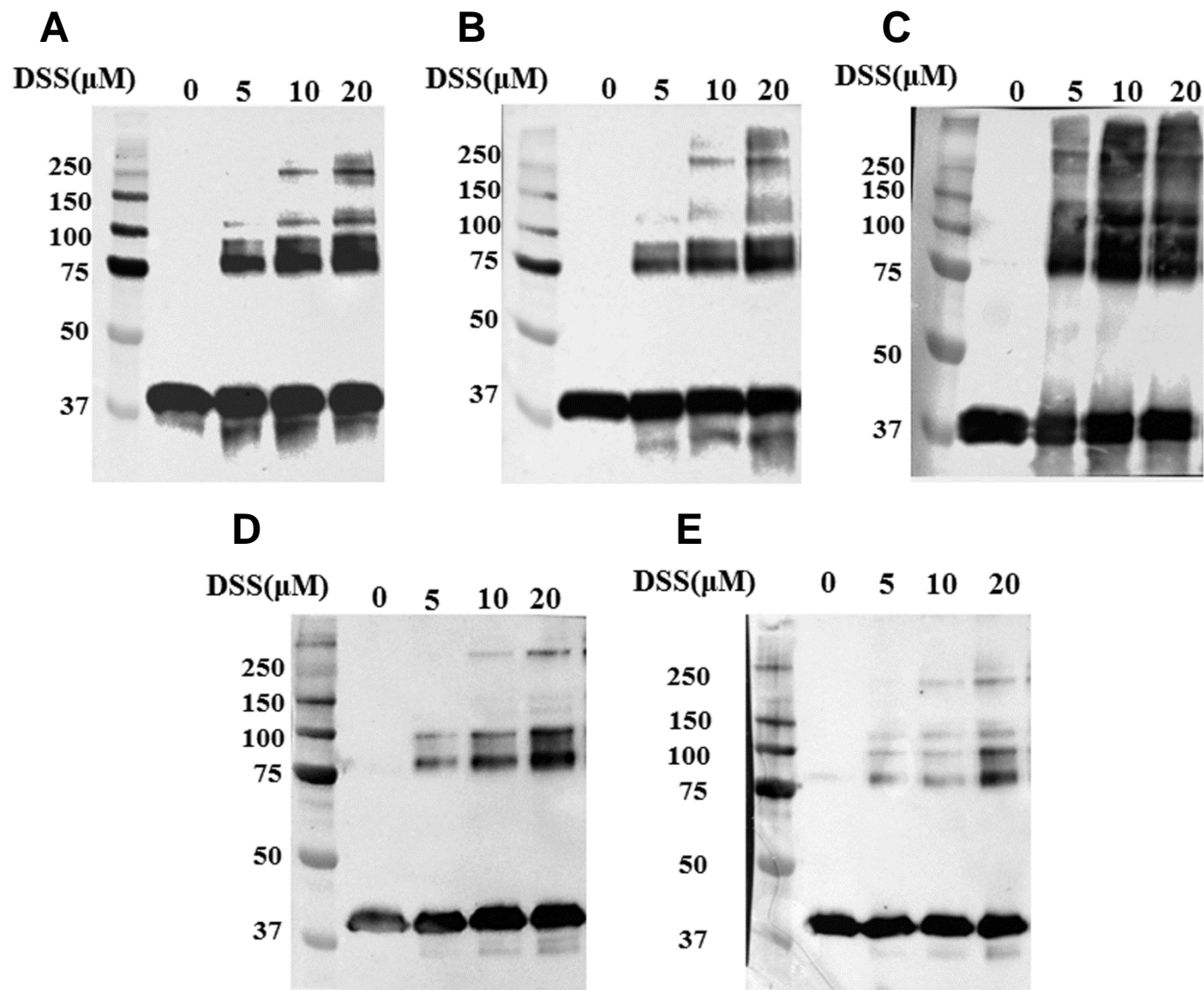


Figure 4

Peak	Sample	Elution Volume (ml)	MW(kDa)
Red	Cag α	1.74	244.1
Blue	Cag α +ATP- γ -S	1.74	244.1
Green A	Cag α +1G2	1.83	175.5
Green B	Cag α +1G2	2.14	54

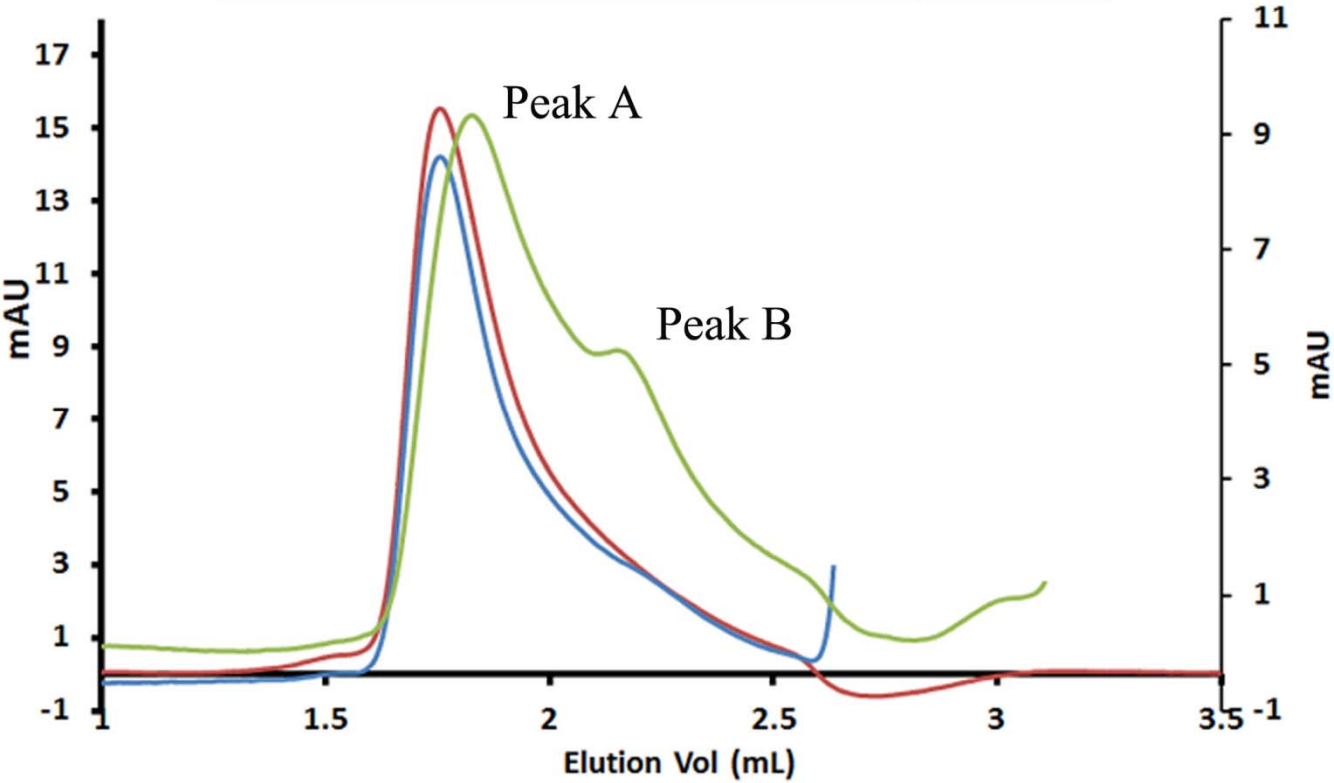


Figure 5

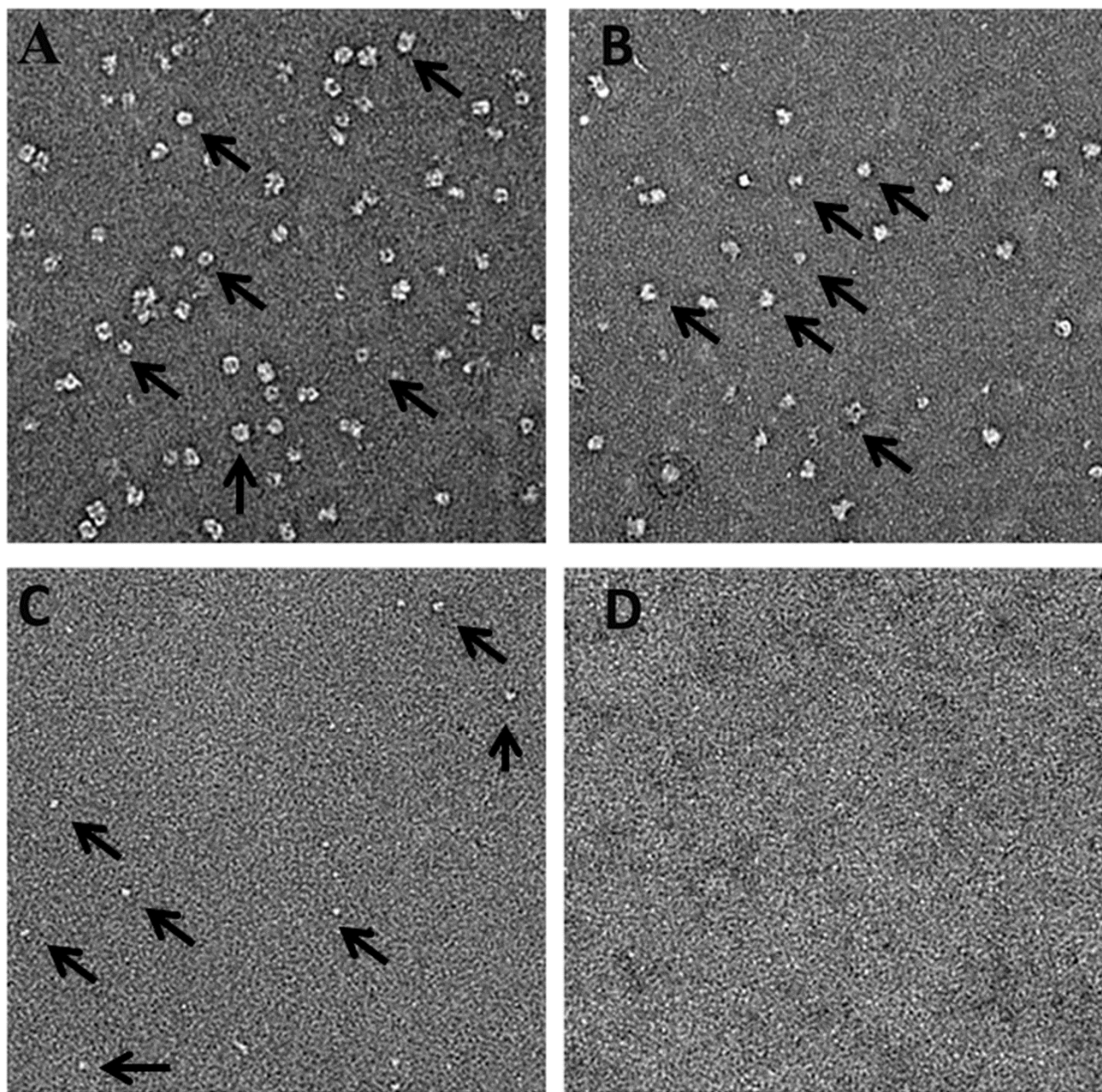


Figure 6

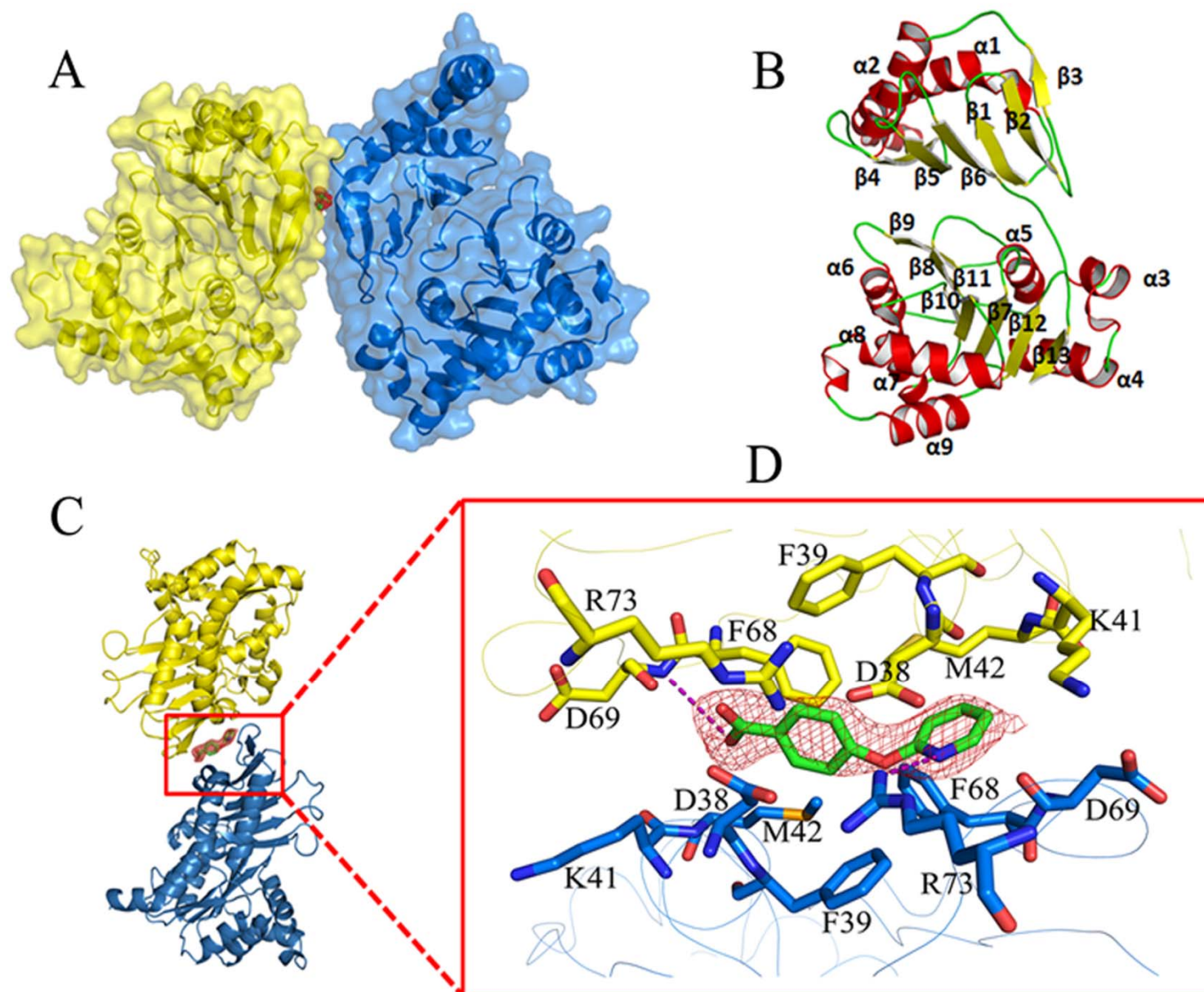


Figure 7

